

RESEARCH ARTICLE

# Trajectory planning of a 4-RR(SS)<sub>2</sub> high-speed parallel robot

Huipu Zhang<sup>1</sup>, Manxin Wang<sup>1,\*</sup> , Haibin Lai<sup>1</sup> and Junpeng Huang<sup>2</sup>

<sup>1</sup>School of Mechanical Engineering, Nanjing University of Science and Technology, Nanjing 210094, China and

<sup>2</sup>Lianyungang Screws Robot Technology Co., Ltd, Lianyungang 222062, China

\*Corresponding author. E-mail: mxwang@njust.edu.cn

**Received:** 14 April 2021; **Revised:** 1 December 2021; **Accepted:** 2 December 2021; **First published online:** 7 January 2022

**Keywords:** high-speed parallel robot, trajectory planning, Lamé curve

## Abstract

The trajectory-planning method for a novel 4-degree-of-freedom high-speed parallel robot is studied herein. The robot's motion mechanism adopts RR(SS)<sub>2</sub> as branch chains and has a single moving platform structure. Compared with a double moving platform structure, the proposed parallel robot has better acceleration and deceleration performance since the mass of its moving platform is lighter. An inverse kinematics model of the mechanism is established, and the corresponding relationship between the motion parameters of the end-moving platform and the active arm with three end-motion laws is obtained, followed by the optimization of the motion laws by considering the motion laws' duration and stability. A Lamé curve is used to transition the right-angled part of the traditional gate trajectory, and the parameters of the Lamé curve are optimized to achieve the shortest movement time and minimum acceleration peak. A method for solving Lamé curve trajectory interpolation points based on deduplication optimization is proposed, and a grasping frequency experiment is conducted on a robot prototype. Results show that the grasping frequency of the optimized Lamé curve prototype can be increased to 147 times/min, and its work efficiency is 54.7% higher than that obtained using the traditional Adept gate-shaped trajectory.

## 1. Introduction

A high-speed parallel robot that is driven by external rotation and contains parallelogram branch chains is a type of industrial robot in which the driver can be placed on the fixed base and the follower arm can be designed as a light rod; this enables the end effector obtaining high speed and acceleration in the process, which is particularly suitable for sorting, handling and picking, and placing of light objects on high-speed logistics production lines. Typical examples of this kind of parallel robot are H4, I4, X4, and PAR4 [1–4]. These robots have been widely used in automated production lines in food, electronics, medicine, and other light industries [5].

High-speed pick-and-place operations require the end effector of the parallel robot to move at a high speed and acceleration. If the motion function and trajectory path of the end-moving platform of the mechanism are not properly selected, there will be abrupt changes in the position, speed, and acceleration during the movement, resulting in unstable motion, affecting the operation and quality of the pick-and-place operation as well as the service life of the parallel robot. However, the sole pursuit of a smooth trajectory will decrease the efficiency. Trajectory planning can determine the optimal solution that considers both the motion function and trajectory path; therefore, it is crucial in the development of motion control for a high-speed parallel robot parallel.

Two approaches are broadly used to improve robot work efficiency based on trajectory planning: trajectory path optimization and motion function optimization. The high-speed parallel robot's pick-and-place trajectory is generally gate-shaped. Optimizing the right-angled part between its vertical motion and horizontal motion is the key to improving motion efficiency. Thus far, various paths have been

proposed to transition the right-angled part of the gate-shaped trajectory, such as the use of straight-arc line [6], which has higher work efficiency than the elliptic trajectory but has the disadvantage of a sudden change in normal acceleration. The fifth-degree polynomial curve [7] and Lamé curve (super elliptic curve) [8–9] can effectively avoid abrupt changes because their acceleration curvatures are continuous; however, the calculation of the path interpolation point is more complicated. In order to reduce the mathematical complexity, Mahmood et al. proposed an new algorithm for smooth trajectory planning optimization of isotropic translational parallel manipulators by using fifth-order B-Splines [10]. The use of spiral-circular curve [11] also can avoid this sudden change in the normal acceleration in the gate-shaped trajectory; however, the choice of the motion law is relatively limited; the Pythagorean hodographs curve [12–14] can be used to optimize the trajectory to minimize the pick-and-place operation cycle, which not only improves the efficiency but also obtains a smooth motion trajectory. In addition, some scholars consider an optimal path tracking formulation focusing on multi-objective optimization without violating the kinematic constraints [15–16]. And several attempts have been made to smoothen the transition at the combination of linear interpolation by using Lamé curve trajectory while without considering the influence of the end-motion law and the motion trajectory on the joint motion of the active arm [17]. Although the above-mentioned methods can obtain smooth transition curves, the calculation of path interpolation points is complicated. Moreover, these methods may lack the exquisiteness of the motion law or have the disadvantage of flexible impact. Presently, the optimization of the motion function mainly involves the parameter optimization of single motion law with the shortest time as the goal, such as optimizing the running time using a genetic algorithm [18–20] and reducing the maximum angular acceleration of the shaft end by changing the motion law parameters [21–22].

This study employs a novel 4-DOF high-speed parallel robot proposed by Nanjing University of Science and Technology as the object [23], establishes its kinematics model, and then starts with the motion function and trajectory path optimization, focusing on the motion state of the active arm. Furthermore, the problem of robot motion trajectory planning to improve the stability and rapidity of the high-speed parallel robot's pick-and-place operation is investigated herein.

## 2. System description

Figure 1 shows the three-dimensional (3D) view of the 4-RR(SS)<sub>2</sub> four-DOF high-speed parallel robot mechanism. The mechanism mainly includes a static platform, a moving platform, and four branch chains connecting the static and moving platforms with the same structure. Each branch chain comprises a rotating fork, an active arm, and a follower arm containing a parallelogram. The type of the chain is RR(SS)<sub>2</sub>, where R represents the rotating pair, R represents the active rotating pair, and (SS)<sub>2</sub> represents a parallelogram structure with a spherical joint at both ends. The branch chain with R(SS)<sub>2</sub> as the topological structure has a 3D translation. Thus, each branch chain is connected to the static platform by a rotating fork, that is, each branch chain is added with a rotating pair, which is why each branch chain has the ability of 3D translation and one-dimensional rotation. As the rotation axes of the rotation pairs added by the four branch chains are parallel to the vertical axis, the moving platform can three-dimensionally translate and rotate around the vertical axis. Notably, to provide the rotational torque around the vertical axis, the four branch chains are designed as offset structures and the movable platform is designed as a nonsquare structure. Owing to the single-action platform structure of the robot, the weight of moving parts can be effectively reduced, improving the dynamic characteristics of the robot and allowing high speed and acceleration. Compared with X4 parallel manipulator (which is a R(SS)<sub>2</sub>R parallel manipulator) [24], the difference lies in the position setting of revolute pairs with axes parallel to each other. The proposed parallel manipulator may be able to further decrease the size of the moving platform since the revolute pairs are moved from being connected with the moving platform to being connected with the static platform. This is beneficial to improve the acceleration and deceleration performance of the mechanism.

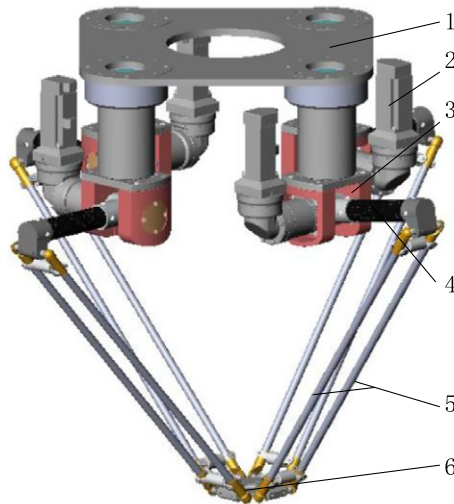


**Figure 1.** Model of 4-RR(SS)2 high-speed parallel robot. 1. Static platform 2. Servo motor 3. Rotating fork. 4. Active arm 5. Follower arm 6. Moving platform.

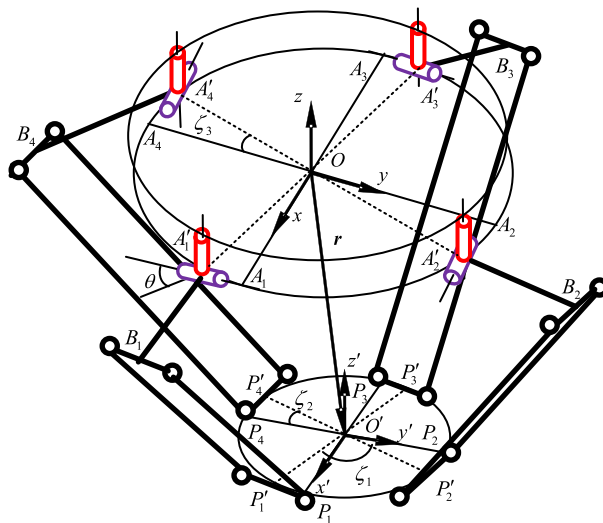


**Figure 2.** Schematic of the organization.

Figure 2 shows the structure of the mechanism. In Fig. 2,  $P'_i$  and  $A'_i$  ( $i = 1, 2, 3, 4$ ) are the hinge centers connecting the branch chain  $i$  and the moving and static platforms, respectively;  $B_i$  is the hinge center connecting the active arm and the follower arm. Let  $A_i$  and  $P_i$  be the positions before the offset of the branches of  $A'_i$  and  $P'_i$ . A fixed reference coordinate system  $O - xyz$  is established with the geometric center point of the stationary platform as the origin, where the  $x$ -axis direction points from point  $O$  to point  $A_1$ ,  $z \perp A_1A_2A_3A_4$ , and the  $y$ -axis satisfies the right-hand rule. In the initial position, the centerlines of the R turning pairs on  $A'_3$  and  $A'_1$  are still parallel to the  $y$ -axis after offset installation and the center lines of the R turning pairs on  $A'_4$  and  $A'_2$  are still parallel to the  $x$ -axis after offset installation. The geometric center point of the moving platform is considered as the origin to construct the moving platform conjoined coordinate system  $O' - x'y'z'$ , where the  $x$ -axis direction points from point  $O'$  to point  $P_1$ ,  $z' \perp P_1P_2P_3P_4$ , and the  $y$ -axis satisfies the right-hand rule. For the convenience of description, here,  $\zeta_1$

is the structural angle of the moving platform, that is, the obtuse angle between  $\overline{P_1P_3}$  and  $\overline{P_2P_4}$ , and  $\zeta_2$  and  $\zeta_3$  are the assembly offset angles of the moving and static platforms, respectively, that is, the acute angles between  $P_1P_3$  and  $\overline{P_1P_3}$  and between  $A_1A_3$  and  $\overline{A_1A_3}$ , respectively.

### 3. Kinematics modeling

As shown in Fig. 2, the position vector of the reference point  $O'$  of the moving platform in the reference coordinate system  $O - xyz$  can be expressed as

$$\mathbf{r} = \mathbf{a}_i + L_1\mathbf{u}_i + L_2\mathbf{w}_i - \mathbf{p}_i, \quad i = 1, 2, 3, 4 \tag{1}$$

where  $L_1$  and  $L_2$  are the rod lengths of the active arm and the follower arm, respectively,  $\mathbf{u}_i$  and  $\mathbf{w}_i$  are their unit direction vectors, and  $\mathbf{a}_i$  and  $\mathbf{p}_i$  are the position vectors from point  $O$  to  $A_i$  and  $O'$  to  $P_i$ , respectively. Furthermore,  $\mathbf{a}_i = R_1(\cos(\gamma_i + \zeta_3)\sin(\gamma_i + \zeta_3)\mathbf{0})^T$ ,  $\mathbf{u}_i = (\cos(\theta + \gamma_i)\cos\alpha_i\sin(\theta + \gamma_i)\cos\alpha_i - \sin\alpha_i)^T$ ,  $\gamma_i = (i - 1)\pi/2$ ,  $\mathbf{p}_i = R_2(\cos\beta_i\sin\beta_i\mathbf{0})^T$ ,  $\beta_i = (i - 1 - \varepsilon_i)\pi/2 + \varepsilon_i\zeta_1 + \zeta_2 + \theta$ ,  $\varepsilon_i = \begin{cases} 0, & i = 1, 3 \\ 1, & i = 2, 4 \end{cases}$ ,  $R_1$  and  $R_2$  are the radii of the moving and static platform, respectively,  $\alpha_i$  is the rotation angle of the active arm, and  $\gamma_i$  is the azimuth angle of  $A_i$ .  $\theta$  is the rotation angle around the  $z$ -axis when the mechanism moves.

Combining Eq. (1) and 4-RR(SS)<sub>2</sub> mechanism characteristics can be obtained as

$$\alpha_i = 2 \arctan \frac{A_i \pm \sqrt{A_i^2 + B_i^2 - C_i^2}}{B_i^2 - C_i^2} \tag{2}$$

$$\mathbf{w}_i = \frac{\mathbf{r} + \mathbf{p}_i - \mathbf{a}_i - L_1\mathbf{u}_i}{L_2} \tag{3}$$

where  $A_i = 2L_1m_{iz}$ ,  $B_i = -2L_1m_{ix}\cos(\theta + \gamma_i) + 2L_1m_{iy}\sin(\theta + \gamma_i)$ , and  $C_i = |m_i|^2 + L_1^2 - L_2^2$ ;  $i = 1, 2, 3, 4$ ,  $\pm$  are determined according to the initial configuration of the mechanism:

Derivation of Eq. (1) leads to

$$\dot{\mathbf{r}} = L_1(\boldsymbol{\omega}_{1i} \times \mathbf{u}_i) + L_2(\boldsymbol{\omega}_{2i} \times \mathbf{w}_i) - \dot{\theta}\hat{\mathbf{z}} \times \mathbf{p}_i \tag{4}$$

where  $\dot{\mathbf{r}}$  represents the linear velocity of point  $O'$  of the moving platform.  $\boldsymbol{\omega}_{1i}$  and  $\boldsymbol{\omega}_{2i}$  represent the angular velocity of the active arm and the follower arm, respectively.  $\dot{\theta}$  is the angular velocity of the rotating fork around the vertical axis,  $\hat{\mathbf{z}}$  is the  $z$ -axis unit direction vector,  $\boldsymbol{\omega}_{1i} = \dot{\theta}\hat{\mathbf{z}} + \dot{\alpha}_i\mathbf{v}_i$ ,  $\dot{\alpha}_i$  is the angular velocity of the active arm relative to the rotating fork,  $\mathbf{v}_i$  is the unit vector of the axis, where the active **R** pair is located, which can be expressed as  $\mathbf{v}_i = (-\sin(\theta + \gamma_i)\cos(\theta + \gamma_i)\mathbf{0})^T$ . By multiplying both sides of Eq. (4) by  $\mathbf{w}_i$  and arranging them into a matrix form, we obtain

$$\dot{\boldsymbol{\alpha}} = \mathbf{J}\dot{\mathbf{x}}, \tag{5}$$

$$\dot{\boldsymbol{\alpha}} = (\dot{\alpha}_1\dot{\alpha}_2\dot{\alpha}_3\dot{\alpha}_4)^T,$$

$$\dot{\mathbf{x}} = (\dot{\mathbf{r}}^T\dot{\theta})^T, \quad \mathbf{J} = \mathbf{J}_q^{-1}\mathbf{J}_x, \quad \mathbf{J}_q = \text{diag}(L_1\mathbf{w}_i^T(\mathbf{v}_i \times \mathbf{u}_i)), \quad \mathbf{J}_x = \begin{bmatrix} \mathbf{w}_1^T & \mathbf{w}_1^T(\hat{\mathbf{z}} \times (L_1\mathbf{u}_1 - \mathbf{p}_1)) \\ \mathbf{w}_2^T & \mathbf{w}_2^T(\hat{\mathbf{z}} \times (L_1\mathbf{u}_2 - \mathbf{p}_2)) \\ \mathbf{w}_3^T & \mathbf{w}_3^T(\hat{\mathbf{z}} \times (L_1\mathbf{u}_3 - \mathbf{p}_3)) \\ \mathbf{w}_4^T & \mathbf{w}_4^T(\hat{\mathbf{z}} \times (L_1\mathbf{u}_4 - \mathbf{p}_4)) \end{bmatrix}$$

where  $\mathbf{J}_q$  and  $\mathbf{J}_x$  represent the direct and indirect Jacobian matrix, respectively, and  $\mathbf{J}$  represents the Jacobian matrix, which represents the mapping relationship between the end speed and that of the active joint.

Taking the derivative of Eq. (4) gives

$$\ddot{\mathbf{r}} = L_1\dot{\boldsymbol{\omega}}_{1i} \times \mathbf{u}_i + L_1\boldsymbol{\omega}_{1i} \times (\boldsymbol{\omega}_{1i} \times \mathbf{u}_i) + L_2\dot{\boldsymbol{\omega}}_{2i} \times \mathbf{w}_i + L_2\boldsymbol{\omega}_{2i} \times (\boldsymbol{\omega}_{2i} \times \mathbf{w}_i) - [\dot{\boldsymbol{\omega}} \times \mathbf{p}_i + \boldsymbol{\omega} \times (\boldsymbol{\omega} \times \mathbf{p}_i)]. \tag{6}$$

Substituting the derivative of  $\omega_{1i}$  and  $\omega$  into Eq. (6), then taking the dot product on both sides of Eq. (6) with  $w_i$ , and arranging them into a matrix form yields

$$\ddot{\alpha} = J\ddot{x} + f(\dot{x}), \tag{7}$$

where  $\ddot{\alpha} = (\ddot{\alpha}_1 \ddot{\alpha}_2 \ddot{\alpha}_3 \ddot{\alpha}_4)^T$ ,  $\ddot{x} = (\ddot{r}^T \ddot{\theta})^T$ ,  $f = (f_1 f_2 f_3 f_4)^T$ ,  $f_i = \dot{x}^T H_i \dot{x} / L_1^2$ ,

$$H_i = U_i \left( Q_i + L_1 w_i \cdot u_i J_{\omega 1i}^T J_{\omega 1i} + \frac{1}{L_2} J_{\omega 2i}^T J_{\omega 2i} \right), \quad U_i = \frac{L_1}{w_i \cdot [v_i \times u_i]}, \quad J_{\omega 1i} = (\hat{z} [0001] + v_i J_i), \quad \text{and}$$

$$J_{\omega 2i} = \frac{1}{L_2} [w_i \times] \left( [E_3 (L_1 u_i - p_i) \times \hat{z}] - L_1 (v_i \times u_i) J_i \right) Q_i = \begin{bmatrix} 0 & 0 & 0 & L_1 J_{i1} \dot{v}'_i \cdot [w_i \times u_i] \\ 0 & 0 & 0 & L_1 J_{i2} \dot{v}'_i \cdot [w_i \times u_i] \\ 0 & 0 & 0 & L_1 J_{i3} \dot{v}'_i \cdot [w_i \times u_i] \\ 0 & 0 & 0 & L_1 J_{i4} \dot{v}'_i \cdot [w_i \times u_i] - w_i \cdot p_i \end{bmatrix},$$

where  $J_i$  represents the row vector of the  $i$ th row of  $J$ .

### 4. Motion law optimization

From the cam design theory, common motion laws include sinusoidal acceleration, modified trapezoidal acceleration, and 3-4-5 polynomials [25]. To obtain the optimal motion law suitable for the 4-RR(SS)<sub>2</sub> parallel mechanism, the above-mentioned three motion laws are compared and analyzed. The variation law of 3-4-5 polynomial acceleration  $a_{345}$ , sinusoidal acceleration  $a_{\sin}$ , and modified trapezoidal acceleration  $a_{MT}$  with time  $t$  can be expressed as follows:

$$a_{345}(t) = \frac{a_{\max}}{5.7735} \left[ 60 \left( \frac{t}{T_{345}} \right) - 180 \left( \frac{t}{T_{345}} \right)^2 + 120 \left( \frac{t}{T_{345}} \right)^3 \right], \tag{8}$$

$$a_{\sin}(t) = a_{\max} \sin \left( \frac{2\pi}{T_{\sin}} \cdot t \right), \tag{9}$$

$$a_{MT}(t) = \begin{cases} a_{\max} \sin(4\pi t / T_{MT}) & (0 \leq t \leq 0.125T_{MT}) \\ a_{\max} & (0.125T_{MT} < t \leq 0.375T_{MT}) \\ a_{\max} \cos[4\pi(t - 0.375T_{MT}) / T_{MT}] & (0.375T_{MT} < t \leq 0.625T_{MT}) \\ -a_{\max} & (0.625T_{MT} < t \leq 0.875T_{MT}) \\ -a_{\max} \cos[4\pi(t - 0.875T_{MT}) / T_{MT}] & (0.875T_{MT} < t \leq T_{MT}) \end{cases}, \tag{10}$$

where  $a_{\max}$  represents the maximum acceleration and  $T_{345}$ ,  $T_{\sin}$ , and  $T_{MT}$  are the periods of the three laws of motion.  $S$  is defined as the total length of the motion path, and the periods of the three motion laws can be calculated as follows:

$$T_{345} = \sqrt{\frac{5.7735S}{a_{\max}}} T_{\sin} = \sqrt{\frac{2\pi S}{a_{\max}}} T_{MT} = \sqrt{\frac{4.889S}{a_{\max}}} \tag{11}$$

The selection criterion of the movement law is whether the movement is fast and stable. It can be assessed by comparing the movement period  $T$ , acceleration peak  $a_{\max}$ , and jump peak  $j_{\max}$  under the same path  $S$ . The smaller the  $a_{\max}$  and  $j_{\max}$ , the more stable is the movement of the mechanism. The formula of the index  $j_{\max}$  is as follows:

$$j_{\max} = C_j S \frac{1}{T^3} \tag{12}$$

where  $C_j$  is the characteristic coefficient. The characteristic coefficients  $C_j$  of the 3-4-5 polynomial, sine acceleration, and modified trapezoidal acceleration are 60, 39.5, and 61.4, respectively.

The typical pick-and-place operation path of a high-speed parallel robot is the Adept gate-shaped trajectory, as shown in Fig. 3, where the AB and CD sections represent the vertical motions and the BC section represents the horizontal motions. Without loss of generality, segments AB and BC are considered motion trajectories to optimize the above-mentioned three motion laws. In this case, the

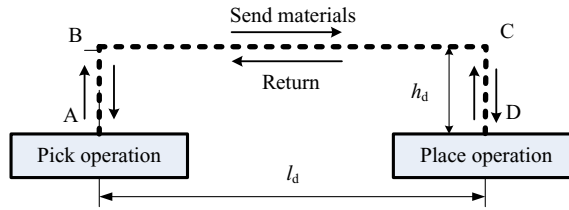


Figure 3. Adept door-shaped trajectory.

acceleration peak value  $a_{max}$  is set to  $50 \text{ m/s}^2$ , the vertical displacement of section AB is  $0.025 \text{ m}$ , and the horizontal displacement of section BC is  $0.30 \text{ m}$ .

Tables I and II show the peak value and time of jump at the end reference point and active arm joint, respectively, when the end trajectory is segment AB. Tables III and IV show the peak value and time of jump at the end reference point and active arm joint when the end trajectory is the BC segment, respectively.

Under the same terminal acceleration peak condition, irrespective of whether the mechanism performs a horizontal or vertical movement, the modified trapezoidal movement law takes the shortest time. Therefore, in the pursuit of high-speed parallel mechanism trajectory-planning research, the modified trapezoidal motion law can be used to achieve the highest frequency motion. At the same time, when the modified trapezoidal motion law is adopted, the peak value of the jerk at the end reference point is 2.26 times that of the sine function and 1.31 times that of the 3-4-5 degree polynomial. For the active arm, the peak angular acceleration of the modified trapezoidal motion law is also the highest, implying that the motion is unstable. Although the sine function motion law can minimize the peak value of the jump, the motion efficiency is also the lowest. Therefore, considering the length and stability of the motion, the 3-4-5 degree polynomial is selected as the motion law of the end trajectory of the mechanism.

## 5. Motion path planning

### 5.1. Gate-shaped trajectory

A typical Adept gate-shaped trajectory model comprises three straight lines, as shown in Fig. 3, where the lifting height  $h_d = 25 \text{ mm}$  and the horizontal movement distance  $l_d = 300 \text{ mm}$ . If the 3-4-5 polynomial motion law is applied to the entire gate-shaped trajectory path, the total length of the path is

$$S_d = 2h_d + l_d, \tag{13}$$

As shown in Fig. 4, assuming that the peak acceleration  $a_{max}$  of the  $4\text{-RR}(\text{SS})_2$  parallel mechanism running along the Adept gate-shaped trajectory is  $50 \text{ m/s}^2$ , the angle, angular velocity, and angular acceleration changes of the four active arms of the mechanism can be obtained using the inverse solution model.

Figure 4 shows that when the end of the mechanism runs along the Adept gate-shaped trajectory, the angular accelerations of the four active arms experience abrupt changes in the orthogonal turning point. The rapid changes in the active joints during high-speed movement will have a greater impact on the mechanism. If stopping and restarting at right angles for stability causes the motion cycle to increase considerably, considering the Adept gate-shaped trajectory, the Lamé curve is used to transition the right-angled part.

### 5.2. Lamé trajectory

Circular arc transition is a traditional approach of transitioning right-angled parts; however, often because of an abrupt change in curvature at the intersection of the straight line and circular arc, it causes

**Table I.** Simulation results of extremity motion parameters in a vertical trajectory.

Law	Displacement/m	$a_{\max}/(m/s^2)$	Time/s	Peak jerk
3-4-5	0.025	50	0.054	$9.671 \times 103$
Sine	0.025	50	0.056	$5.608 \times 103$
Correct trapezoid	0.025	50	0.049	$12.701 \times 103$

**Table II.** Simulation results of active arm-motion parameters during vertical trajectory.

Law	Angle/ $^\circ$	Max angular acceleration/ $(^\circ/s^2)$	Time/s	Max angular velocity/ $(^\circ/s)$
3-4-5	8.78	$18.256 \times 103$	0.054	306.2
Sine	8.78	$18.088 \times 103$	0.056	313.1
Correct trapezoid	8.78	$18.575 \times 103$	0.049	354.8

**Table III.** Simulation results of terminal motion parameters in a horizontal trajectory.

Law	Displacement/m	$a_{\max}/(m/s^2)$	Time/s	Peak jerk
3-4-5	0.30	50	0.186	$2.792 \times 103$
Sine	0.30	50	0.194	$1.619 \times 103$
Correct trapezoid	0.30	50	0.171	$3.666 \times 103$

**Table IV.** Simulation results of active arm-motion parameters in a horizontal trajectory.

Law	Angle/ $^\circ$	Max angular acceleration/ $(^\circ/s^2)$	Time/s	Max angular velocity/ $(^\circ/s)$
3-4-5	61.29	$12.433 \times 103$	0.186	713.3
Sine	61.29	$12.398 \times 103$	0.194	728.8
Correct trapezoid	61.29	$15.047 \times 103$	0.171	823.6

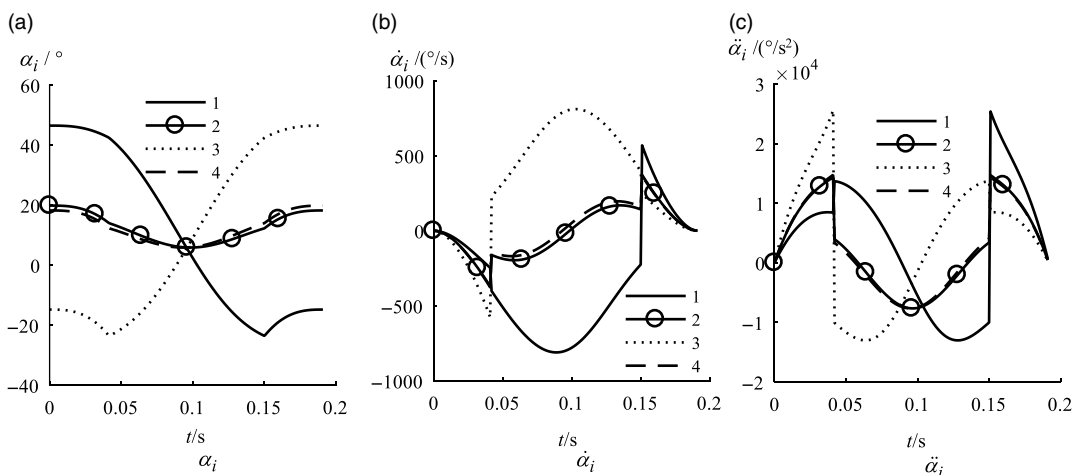


**Figure 4.** Changes in the angle, angular velocity, and angular acceleration of the driving arm in the adept gate path (1, 2, 3, and 4 represent the label of the driving arm).

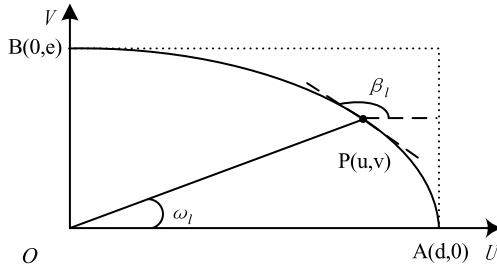


Figure 5. Lamé curve.

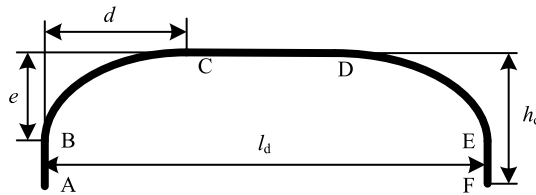


Figure 6. Adept gate-shaped trajectory after Lamé curve transition.

a sudden centripetal acceleration, shaking the end-moving platform. A Lamé curve is also called a super elliptic curve because it exhibits curvature continuity, which is why it can avoid the impact of centripetal acceleration caused by sudden curvature in the trajectory.

As shown in Fig. 5, the Lamé curve is analyzed in the first quadrant, and its trajectory satisfies Eq. (14):

$$\left(\frac{u}{d}\right)^3 + \left(\frac{v}{e}\right)^3 = 1, \tag{14}$$

where  $d$  is the long axis length and  $e$  is the short axis length.

To calculate the new trajectory length, the length of the Lamé curve  $\widehat{APB}$  needs to be calculated first. In the coordinate system  $O-uv$ , the coordinate of point  $P$  can be expressed as

$$u(\omega_l) = \frac{d}{\left(1 + \left(\frac{d}{e} \tan(\omega_l)\right)^3\right)^{\frac{1}{3}}}, \quad v(\omega_l) = \frac{d \tan(\omega_l)}{\left(1 + \left(\frac{d}{e} \tan(\omega_l)\right)^3\right)^{\frac{1}{3}}}, \tag{15}$$

where  $\omega_l$  represents the angle between  $\widehat{OP}$  and  $U$  axis,  $\beta_l$  represents the cut angle.

According to the arc length formula,  $\widehat{AP}$  is expressed as

$$AP = \int_0^{\omega_l} \left\{ \left[ \left( \frac{d(\tan^2 \omega_l + 1)}{\left(\left(\frac{d}{e} \tan \omega_l\right)^3 + 1\right)^{\frac{1}{3}}} \right)^2 - \frac{d^4 \tan^3 \omega_l (\tan^2 \omega_l + 1)}{e^3 \left(\left(\frac{d}{e} \tan \omega_l\right)^3 + 1\right)^{\frac{4}{3}}} \right]^2 + \frac{d^8 \tan^4 \omega_l (\tan^2 \omega_l + 1)^2}{e^6 \left(\left(\frac{d}{e} \tan \omega_l\right)^3 + 1\right)^{\frac{5}{3}}} \right\}^{\frac{1}{2}} d\omega_l, \tag{16}$$

As shown in Fig. 6, the length of the entire path can be obtained:

$$S_{Lame} = 2h_d + l_d - 2(d + e) + BC + DE, \tag{17}$$

If the total length of the path is known, the total time  $T$  through the entire path can be obtained from Eq. (11). Furthermore, the total length of the gate-shaped trajectory path after the Lamé curve transition depends on the size of the two parameters  $d$  and  $e$  of the Lamé curve. Figure 7 shows the change rule of the total time  $T$  with respect to  $d$  and  $e$  under the 3-4-5 polynomial motion rule. Figure 7 shows that



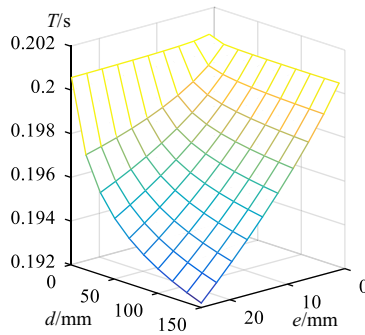


Figure 7. Relationship between total time  $T$  and curve parameters  $d$  and  $e$ .

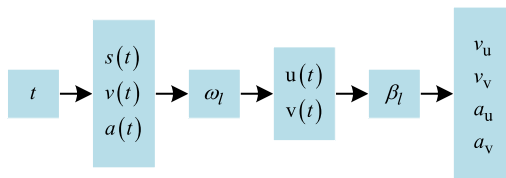


Figure 8. Motion decomposition solution process.

when  $d$  and  $e$  are both 0, that is, when the Lamé curve transition is not used, the gate-shaped trajectory movement time  $T$  is the longest, which is 0.2009 s. The movement duration  $T$  decreases as  $d$  and  $e$  increase. When  $d$  and  $e$  are 150 and 25 mm, respectively, under the gate-shaped trajectory constraint, the total movement duration  $T$  is the shortest, that is, 0.1922 s. There is no straight part on the track at this time.

### 5.3. Motion decomposition

As shown in Fig. 8, according to the 3-4-5 polynomial motion law, the given acceleration peak value, total path length, path length  $s(t)$ , absolute speed  $v(t)$ , and acceleration  $a(t)$  traversed by the end of the mechanism at any  $t$  time can be determined. Based on the arc length formula (20), the angle  $\omega_l$  can be obtained using the inverse solution; then, the velocity ( $v_u, v_v$ ) and acceleration ( $a_u, a_v$ ) in the plane coordinate system  $O$ - $uv$  can be obtained, and further, the velocity ( $v_x, v_y, v_z$ ) and acceleration ( $a_x, a_y, a_z$ ) in the space coordinate system  $O$ - $xyz$  can be obtained by conversion. Owing to the change toward the motion direction, the five-segment route comprising  $\overline{AB}, \overline{BC}, \overline{CD}, \overline{DE}$ , and  $\overline{EF}$  must be decomposed. Furthermore, because the motion solution of the linear part is relatively simple, it will not be explained.

Decomposing the motion on the curve in the coordinate system  $O$ - $uv$  gives

$$\begin{cases} v_u = v(t) \cos \beta_l \\ v_v = v(t) \sin \beta_l \\ a_u = a(t) \cos \beta_l - v(t) \sin \beta_l \frac{d\beta_l}{dt} \\ a_v = a(t) \sin \beta_l + v(t) \cos \beta_l \frac{d\beta_l}{dt} \end{cases} \quad (18)$$

where  $\beta_l$  is the cut angle of the curve in Fig. 5, which can be expressed by the slope of the curve:

$$\tan \beta_l = \frac{dv}{du} = -\frac{e}{d} \left(\frac{u}{d}\right)^2 \left[1 - \left(\frac{u}{d}\right)^3\right]^{-\frac{2}{3}}, \quad (19)$$

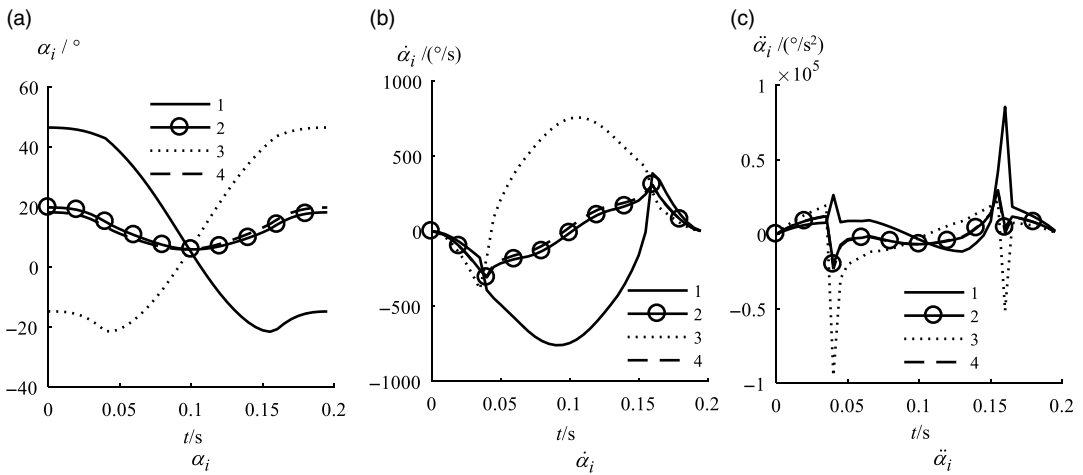


**Figure 9.** Changes in the angle, angular velocity, and angular acceleration of the driving arm under the Lamé trajectory ( $d = 50$  mm and  $e = 10$  mm. 1, 2, 3, and 4 represent the active arm label).

and  $\frac{d\beta_l}{dt}$  can be obtained by deriving the two sides of Eq. (17):

$$\frac{d\beta_l}{dt} = -\cos^2\beta_l (V_1) \frac{du}{dt}, \tag{20}$$

where

$$V_1 = \frac{2eu^4}{d^6 \left(1 - \left(\frac{u}{d}\right)^3\right)^{\frac{5}{3}}} + \frac{2eu}{d^3 \left(1 - \left(\frac{u}{d}\right)^3\right)^{\frac{2}{3}}}. \tag{21}$$

After the two-dimensional motion decomposition of the curve part is obtained, it can be converted into position  $(x, y, z)$ , velocity  $(v_x, v_y, v_z)$ , and acceleration  $(a_x, a_y, a_z)$  in the  $O$ - $xyz$  coordinate system as follows:

$$\begin{cases} x = \cos\theta(u+C_1) \\ y = \sin\theta(u+C_1) \\ z = v+C_2 \end{cases} \quad \begin{cases} v_x = \cos\theta v_u \\ v_y = \sin\theta v_u \\ v_z = v_v \end{cases} \quad \begin{cases} a_x = \cos\theta a_u \\ a_y = \sin\theta a_u \\ a_z = a_v \end{cases} \tag{22}$$

In formula (22),  $C_1$  and  $C_2$  are determined by the size of the curve parameters and specific road section where the end is located.

Figure 9 shows the change in angle, angular velocity, and angular acceleration of the active arm over time when  $a_{\max} = 50$  m/s<sup>2</sup>,  $d = 50$  mm, and  $e = 10$  mm. The figure shows that after the Lamé curve is used to transition the two right angles of the trajectory, compared with the traditional Adept gate-shaped trajectory, the uneven changes in the trajectory of the No. 1 and No. 3 active arm joints at the gate-shaped corners are improved.

In addition, to reveal the influence of the parameters  $d$  and  $e$  of the Lamé curve on the smoothness of motion, Fig. 10 shows the change law of the peak angular acceleration  $\max_i \ddot{\alpha}_i$  of all active arms with respect to  $d$  and  $e$ . Figure 10 shows that  $\max_i \ddot{\alpha}_i$  decreases with increase in  $d$  and  $e$ . When  $d$  has the maximum value of 150 mm (half of the gate-shaped trajectory length  $l_d$ ) and  $e$  has the maximum value of 25 mm (the gate-shaped trajectory height  $h_d$ ), the minimum value of  $\max_i \ddot{\alpha}_i$  is  $2.983 \times 10^4$  °/s<sup>2</sup>. Therefore, to minimize the movement duration  $T$  and the acceleration peak  $\max_i \ddot{\alpha}_i$ , the maximum values for both  $d$  and  $e$  should be substituted, that is,  $d = 150$  and  $e = 25$  mm. The active arm angle, angular velocity, and angular acceleration change laws are shown in Fig. 11. The curve of the motion parameters is smoother, and the peak angular acceleration is reduced. Figure 12 shows the shape of the trajectory path.

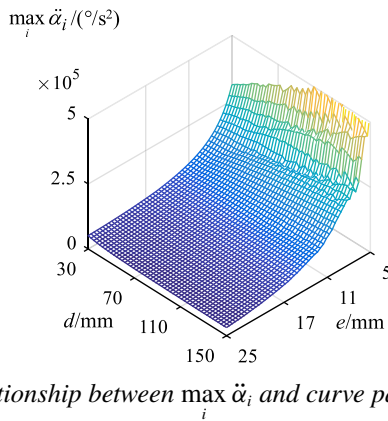


Figure 10. Relationship between  $\max \ddot{\alpha}_i$  and curve parameters  $d$  and  $e$ .

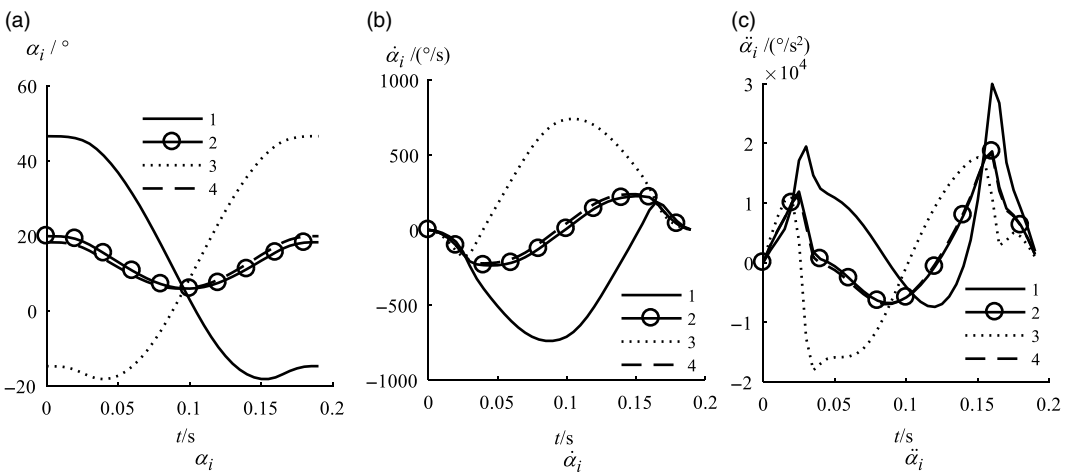


Figure 11. Changes in the angle, angular velocity, and angular acceleration of the driving arm under the Lamé trajectory ( $d = 150$  and  $e = 25$  mm. 1, 2, 3, and 4 represent the active arm label).

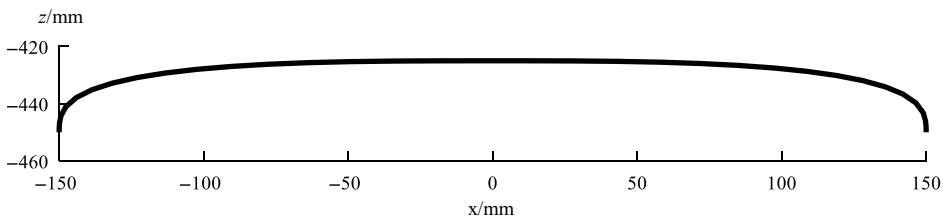


Figure 12. Lamé curve path ( $d = 150$  and  $e = 25$  mm).

## 6. Interpolated motion control

According to previous studies, the Lamé trajectory is less used because the complex arc length given by Eq. (20) must be used to solve the curve angle  $\omega_i$  in reverse when its motion needs to be decomposed. This section solves this problem using numerical solution and deduplication optimization methods.

### 6.1. Interpolation point solution

The Lamé path interpolation program is shown in Fig. 13. First, input parameters such as  $d$ ,  $e$ , and  $a_{\max}$  are used to calculate the total path length  $S$  and the movement duration  $T$  and discretize them. Second,

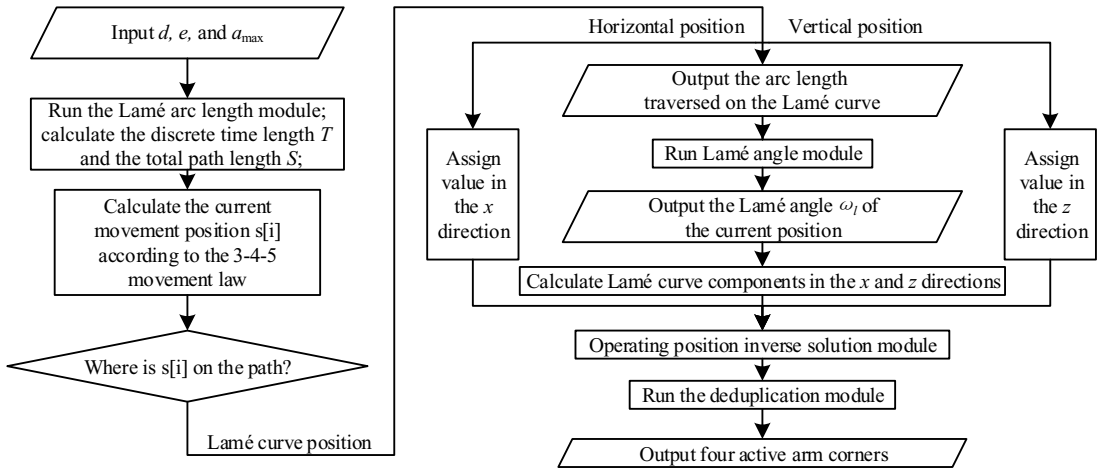


Figure 13. Block diagram of Lamé path interpolation.

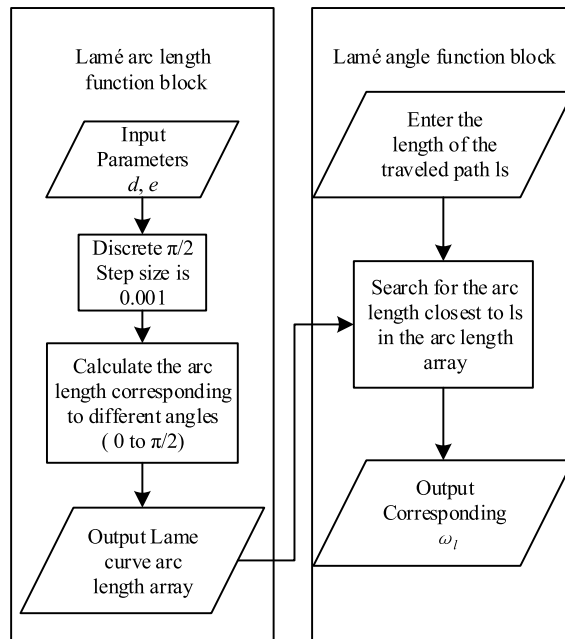


Figure 14. Lamé angle function block and Lamé arc length function block.

according to the selected motion law, the position of the mechanism on the curved track at the current moment of motion is calculated and verified. If it is in the horizontal or vertical position, it can be directly assigned. If it is in the curve position, the angle  $\omega_l$  is obtained using the Lamé angle module and the motion decomposition is completed based on the calculation of the parameter equation. Finally, the position data in the 3D coordinate system  $O-xyz$  obtained after decomposition are subjected to inverse solution and deduplication processing and the interpolation position array of the rotation angle of the active arm can then be outputted.

The angle  $\omega_l$  is calculated using the Lamé arc length function block and the Lamé angle function block, as shown in Fig. 14. The Lamé arc length function block discretizes  $\pi/2$  with a step length of 0.001 and then calculates the arc-length array corresponding to different angles from 0 to  $\pi/2$  using

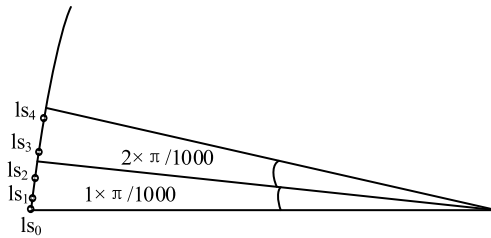


Figure 15. Occurrence of duplicate points.

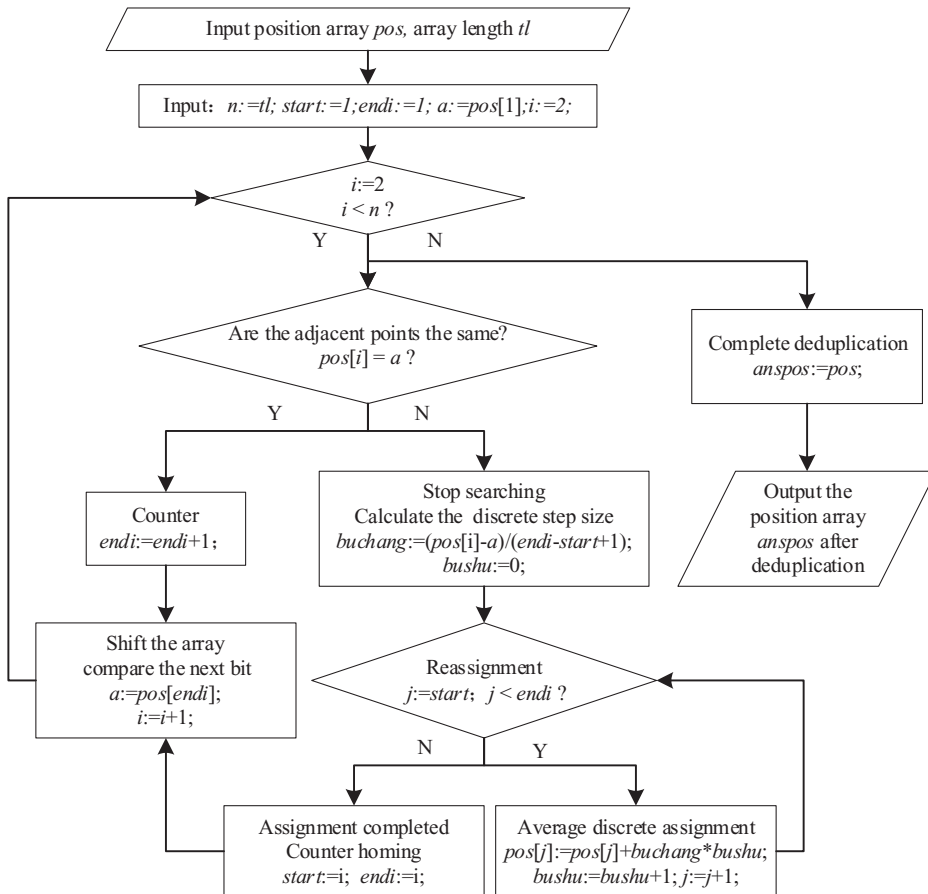
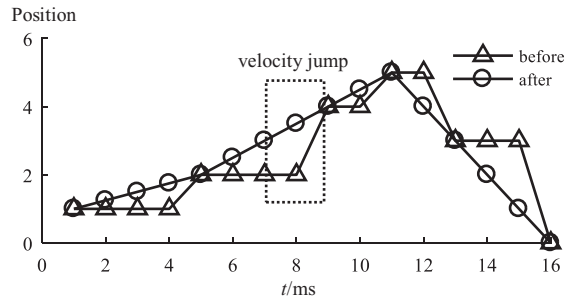


Figure 16. Program block diagram of interpolation point deduplication.

Eq. (17). The Lamé angle function block searches and compares the input total path length  $ls$  at a certain moment with the arc-length array calculated using the arc length module to obtain the arc length closest to the path length  $ls$  and calculates the corresponding angle accordingly.

### 6.2. Deduplication optimization

As shown in Fig. 15, the numerical solution method described above often has duplicate points in the results. As the speed of the parallel robot is extremely slow at the start of the movement, the distance traveled by the mechanism in the first few discrete 1-ms time intervals ( $ls_1$  and  $ls_2$  in the figure) is



**Figure 17.** Interpolation point comparison before and after deduplication.

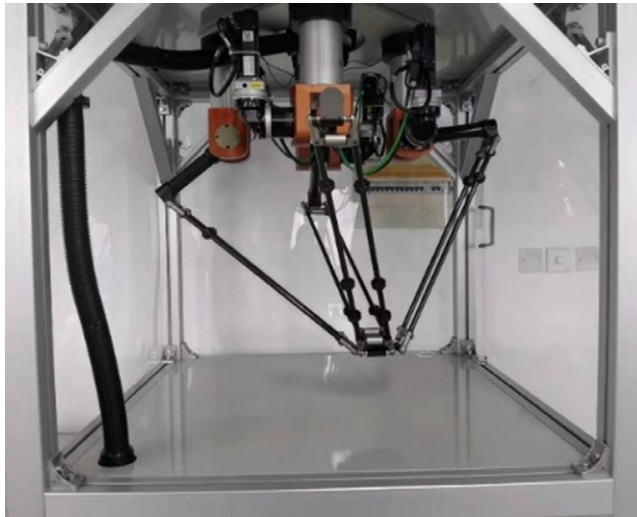


**Figure 18.** Experimental prototype.

frequently smaller than the discrete angular step of the Lamé curve in the program (such as  $\pi/1000$ ). At this time, multiple interpolation points appear in the arc corresponding to the unit discrete angle step. Therefore, the Lamé angle function block will repeatedly identify these interpolation points as the same angle when searching and comparing, resulting in duplicate points in the subsequent solving.

When duplicate points exist in the interpolation point data, the theoretical speed calculated based on the position signal will be inconsistent with the actual speed; the actual speed is always zero at the duplicate point so that the unit discrete angle that was originally set to be completed by multiple interpolation cycles is directly completed only in the last cycle at several times the original speed. Finally, it results in an abrupt change in speed, causing the motor to run unstably and even jitter.

In this case, a part of the duplicate points can be removed by adjusting the difference between the angular and time discrete accuracy; however, this considerably increases the computational burden of the program and does not eliminate the duplicated points.

To completely prevent such situations, an additional function block of interpolation point deduplication is programmed by changing the difference in discrete accuracy, as shown in Fig. 16. After inputting an array with repeated points at the interpolation position, whether the adjacent points of the array are the same is assessed bit by bit. If they are the same, the repeat point counter is incremented and shifted to the next bit to continue the assessment. If the adjacent points are different, the scanning stops. At this time, the value of the duplicate point counter is the step length of the duplicate array segment. Afterward, the identified duplicate array segments are reassigned. Figure 17 shows that after the new assignment,

**Table V.** *Pick-and-place performance experiment (0° direction).*

Direction/°	Acceleration/ (m/s <sup>2</sup> )	cycles/s	Frequency/ (times/min)	Position error (PE)/r	Command speed/(r/min)	Actual current/A
0	10	0.416	69	0.0014	2159	2.1
0	15	0.340	84	0.0019	2681	2.1
0	20	0.295	96	0.018	3051	3.4
0	25	0.263	107	0.0272	3421	3.5
0	30	0.241	116	0.0614	3752	3.5
0	35	0.223	125	0.1031	4034	3.5

**Table VI.** *Pick-and-place performance experiment (45° direction).*

Direction/°	Acceleration/ (m/s <sup>2</sup> )	cycles/s	Frequency/ (times/min)	PE/r	Command speed/(r/min)	Actual current/A
45	10	0.416	69	0.0034	1691	1.5
45	15	0.340	84	0.0039	2098	2.1
45	20	0.295	96	0.0050	2381	2.9
45	25	0.263	107	0.0142	2675	3.3
45	30	0.241	116	0.0165	2909	3.5
45	35	0.223	125	0.0211	3148	3.5
45	40	0.208	133	0.0231	3360	3.5
45	45	0.196	140	0.0754	3518	3.5
45	50	0.186	147	0.1707	3752	3.5

the array segment increases or decreases at a constant speed, eliminating the abrupt change in speed and obtaining an array without duplicate points.

## 7. Experiment

A prototype of the robot is now used to verify the effectiveness of the aforementioned motion trajectory planning and interpolation motion control. Figure 18 shows the test prototype. The control system is TwinCAT 2 from Beckhoff.

In this section, two representative motion directions of 0° and 45° are selected and the robot is allowed to run along the Lamé gate-shaped trajectory with different peak accelerations in the two directions. Simultaneously, the position error (PE), position-to-position velocity command (PTPVCMD), and actual current (IQ) of the motor are recorded during operation to reflect the performance of the mechanism. Referring to the task settings of the ABB Flexpicker manipulator, the round trip is recorded as a pick-and-place operation. The dwell time of the robot during the pick-and-place process is 0.035 s, and then, the pick-and-place frequency per minute can be calculated. The peak acceleration at the end is set to start from 10 m/s<sup>2</sup>, and it gradually increases by 5 m/s<sup>2</sup> to test the pick-and-place frequency and performance of the robot prototype running on the Lamé trajectory.

As shown in Table V, when the robot is running in the 0° direction and the end acceleration is less than 35 m/s<sup>2</sup>, the motor PE is minute and the command speed is also lower than the specified limit. When the end acceleration reaches 35 m/s<sup>2</sup>, the pick-and-place frequency is 125 times/min and the command speed is 4034 r/min, which is close to the maximum motor speed of 5000 r/min. The motor current reaches the current limit value of 3.5 A set by ServoStudio, and its PE exceeds 0.1 r. At this time, increasing the acceleration will cause the driver's power to be insufficient relative to the load and alarm.

As shown in Table VI, compared with the situation when the robot is running in the 0° direction, when the robot is running in the 45° direction, its command speed and current value are reduced. This

is because the robot is mainly powered by only two motors in the  $0^\circ$  direction, and the corresponding active arm has a larger motion range; therefore, the speed will be greater. However, when the robot runs in the  $45^\circ$  direction, the four motors move in the same way and provide power evenly so that the motor speed and current are much smaller and higher command speeds can be achieved, thereby increasing the pick-and-place frequency. When the end acceleration is less than  $50 \text{ m/s}^2$ , the PE is minute, the command speed is also lower than the limit value, and the movement is extremely stable. When the end acceleration reaches  $50 \text{ m/s}^2$ , the pick-and-play frequency is 147 times/min. At this time, although the motor current has reached the set current limit value of 3.5 A and its PE has exceeded 0.1 r, its command speed is only 3752 r/min, which is even lower than that when the robot is running in the  $0^\circ$  direction at  $35 \text{ m/s}^2$ .

The test results show that the prototype adopts the optimized Lamé trajectory-planning method, which can achieve a stable pick-and-place frequency of up to 147 times/min, it is at a level similar to delta and Cross-IV robot [26]. Compared with previous experiments [27], under the same end acceleration, the work efficiency of the traditional Adept gate-shaped trajectory-planning method is improved by 54.7%, and the work efficiency of the arc transition trajectory-planning method is improved by 34.8%. These results verify that the Lamé trajectory-planning method can greatly improve the work efficiency of the mechanism.

## 8. Conclusion

In this study, the trajectory planning of a new type of 4-DOF high-speed parallel robot is investigated. The following conclusions are drawn:

(1) The motion parameters of the end and active arm are compared and analyzed when the mechanism adopts 3-4-5 degree polynomials, sine, and modified trapezoids to run on different trajectories. Then considering the motion time and stability, the optimization of the motion law function is completed.

(2) The influence of different motion paths on the active joints is analyzed, the Lamé curve with continuous curvature is used to replace the original traditional gate-shaped trajectory, and the curve parameters are optimized, enabling the active joint to achieve high-speed and smooth motion.

(3) Propose a method to solve the curve angle  $\omega_i$  in reverse when its motion needs to be decomposed by using numerical solution and deduplication optimization methods.

(4) Experimental results show that the end acceleration of the robot could be as high as  $50 \text{ m/s}^2$ , and the pick-and-place frequency could be as high as 147 times/min, verifying the superiority of the Lamé trajectory-planning method proposed herein.

**Acknowledgements.** This research work is partially supported by the National Natural Science Foundation of China (NSFC) under grants 51605225.

## References

- [1] F. Pierrot and O. Company, "H4: A New Family of 4-DOF Parallel Robots," *Proceedings of the IEEE/ASME International Conference on Advanced Intelligent Mechatronics* (1999) pp. 508–513.
- [2] S. Krut, O. Company, M. Benoit, et al., "I4: A New Parallel Mechanism for SCARA Motions," *Proceedings of the IEEE International Conference on Robotics and Automation* (2003) pp. 1875–1880.
- [3] S. Krut, O. Company, V. Nabat, et al., "Heli4: A Parallel Robot for SCARA Motions with a Very Compact Traveling Plate and a Symmetrical Design," *Proceedings of the IEEE/RSJ International Conference on Intelligent Robots and Systems* (2006) pp. 1656–1661.
- [4] V. Nabat, O. Company, S. Krut, et al., "Par4: Very High Speed Parallel Robot for Pick-and-Place," *Proceedings of the IEEE/RSJ International Conference on Intelligent Robots and Systems* (2005) pp. 1202–1207.
- [5] X. J. Liu, J. S. Wang, et al., "Discussion on new configuration design of parallel robot mechanism," *China Mech. Eng.* **12**(12), 1339–1342 (2001).
- [6] Y. H. Zhu, J. Zhao and H. G. Cai, "Research on the closed-loop self-calibration of delta mechanism," *J. Xi'an Jiaotong Univ.* **8**(2), 134–137 (2005).



- [7] W. Nan, X. Tang and B. Song, "A New Automatic Motion Planning Algorithm for a 4-Degree-of-Freedom Parallel Kinematic Manipulator Based on the Centre Sphere Method," *Proceedings of the Institution of Mechanical Engineers Part B Journal of Engineering Manufacture*. **299**(1), 64–77 (2015).
- [8] Z. X. Xie, D. W. Shang and R. Ren, "Optimization and experimental verification of pick-and-place trajectory for a Delta parallel robot based on lamé curves," *J. Mech. Eng.* **51**(1), 52–59 (2015).
- [9] Z. Y. Zhang, "The research on high-speed motion control for Delta parallel robot," Beijing Jiaotong University (2018).
- [10] W. Chen, Y. Tang and Q. Zhao, "A Novel Trajectory Planning Scheme for Spray Painting Robot with Bézier Curves," 2016 *Chinese Control and Decision Conference (CCDC)* (2016) pp. 6746–6750.
- [11] Y. D. Han, "Path planning and control of Delta robot for high-speed handling," Harbin Institute of Technology (2017).
- [12] T. T. Su and H. J. Zhang et al., "Trajectory planning for a Delta robot based on PH curve," *Robotics* **40**(1), 46–55 (2018).
- [13] J. W. Wu, "Research and design of three-degree-of-freedom Delta robot control system," Qingdao University (2018).
- [14] T. Su, L. Cheng, Y. Wang, X. Liang and H. Zhang, "Time-optimal trajectory planning for delta robot based on quintic pythagorean-hodograph curves," *IEEE Access*. **6**, 28530–28539 (2018).
- [15] X. Luo, S. Li, S. Liu and G. Liu, "An optimal trajectory planning method for path tracking of industrial robots," *Robotica*. **37**(3), 502–520 (2019).
- [16] X. Zhang and G. Shi, "Multi-objective optimal trajectory planning for manipulators in the presence of obstacles," *Robotica*, 1–19 (2021).
- [17] W. Chen, H. Fang, H. E. Wensong, et al., "Optimal trajectory planning with three-parameter Lamé curve for delta robot," *Mach. Des. Res.* **34**(1), 8–12 (2018).
- [18] C. Pan, "Research on trajectory planning and sorting strategy of DELTA parallel robot," Qufu Normal University (2018).
- [19] F. He, "Research on trajectory planning and motion control realization of DELTA parallel robot," Changsha University of Science and Technology (2017).
- [20] M. Cong, Y. K. Xiong, D. Liu and X. L. Yang, "A method of time-optimal trajectories planning for parallel robot operation space," *Mach. Des.* **33**(2), 7–13 (2016).
- [21] J. P. Mei, Y. D. Sun, Y. He, et al. "Trajectory optimization of the 4-DOF parallel manipulator based on the energy-consumption optimization," *Mach. Des.* **345**(7), 17–25 (2018).
- [22] Y. H. Li, "Optimization of delta parallel robot grab and place trajectory," *Electr. Autom.* **38**(3), 20–22 (2016).
- [23] M. X. Wang, T. Huang, H. T. Feng, et al., "A three level one rotation four degree of freedom parallel mechanism," *China Patent* (2015-11-16), ZL201510786414.6.
- [24] F. G. Xie and X. J. Liu, "Design and development of a high-speed and high-rotation robot with four identical arms and a single platform," *ASME J. Mech. Rob.* **7**(4), 041015 (2015).
- [25] X. Zhang, "Research on the Control Method of High Speed Light Parallel Manipulator," Tianjin University (2005).
- [26] S. T. Liu, "Optimal Design of 2-,3-,4-DOF High-speed Parallel Manipulators: Theory and Application," Tianjin University (2012).
- [27] Y. P. Song, "Research on dynamic analysis and motion control of four-degree-of-freedom high-speed parallel robot mechanism," Nanjing University of Science and Technology (2018).